Equilibrium structure of δ-Bi_2O_3 from first principles

2009 J. Phys.: Condens. Matter 21 175403

(http://iopscience.iop.org/0953-8984/21/17/175403)

J. Phys.: Condens. Matter **21** (2009) 175403 (7pp) doi:10.1088/0953-8984/21/17/175403

Equilibrium structure of δ-Bi_2O_3 from first principles

Denis Music[1,3], **Stephanos Konstantinidis**[1,2] **and Jochen M Schneider**[1]

[1] Materials Chemistry, RWTH Aachen University, D-52056 Aachen, Germany
[2] Laboratoire de Chimie Inorganique et Analytique, Université de Mons, Avenue Copernic 1, 7000 Mons, Belgium

E-mail: music@mch.rwth-aachen.de

Received 27 January 2009, in final form 6 March 2009
Published 24 March 2009
Online at stacks.iop.org/JPhysCM/21/175403

Abstract

Using *ab initio* calculations, we have systematically studied the structure of δ-Bi_2O_3 (fluorite prototype, 25% oxygen vacancies) probing ⟨100⟩ and combined ⟨110⟩ and ⟨111⟩ oxygen vacancy ordering, random distribution of oxygen vacancies with two different statistical descriptions as well as local relaxations. We observe that the combined ⟨110⟩ and ⟨111⟩ oxygen vacancy ordering is the most stable configuration. Radial distribution functions for these configurations can be classified as discrete (ordered configurations) and continuous (random configurations). This classification can be understood on the basis of local structural relaxations. Up to 28.6% local relaxation of the oxygen sublattice is present in the random configurations, giving rise to continuous distribution functions. The phase stability obtained may be explained with the bonding analysis. Electron lone-pair charges in the predominantly ionic Bi–O matrix may stabilize the combined ⟨110⟩ and ⟨111⟩ oxygen vacancy ordering.

(Some figures in this article are in colour only in the electronic version)

1. Introduction

Tailoring physical and chemical properties of fast-ion conducting phases is a scientific challenge that may have important environmental and economical impact [1]. Electrolytic fast-ion conducting membranes are active components of sensors, gas exchange membranes and fuel cell devices. In particular, the latter facilitates energy conversion between chemical and electrical energy, being efficient due to its high energy yield and is environmentally friendly [1]. Beside electricity generation, fuel cells produce heat and water. An important step towards efficient energy conversion is the reduction of the operation temperature [2]. This temperature has a strong influence on the conductivity of the electrolytic membranes since electrical conduction is based on the diffusion of ions in these solid. One promising approach to tackle this problem is to use fast-ion conducting thin films, such as metal oxides. Commonly used metal oxide is yttria-stabilized zirconia [2]. δ-Bi_2O_3 is considered to be an important alternative since it possesses the ionic conductivity in the range of 1 S cm^{-1}, approximately two orders of magnitudes larger than the one of yttria-stabilized zirconia at the same temperature [3–5]. Oxygen vacancies intrinsically present in the δ-Bi_2O_3 solid are responsible for its large ionic conductivity [5]. However, its limited thermal stability (between 729 and 835 °C) prevents the use thereof [5]. Therefore, it is necessary to stabilize the δ-Bi_2O_3 structure, for instance by doping or epitaxy, in order to enable fast-ionic conductivity at low temperatures [5, 6].

In order to stabilize δ-Bi_2O_3, it is essential to understand its crystal structure. There are several structural proposals available based on the fluorite prototype (space group $Fm\bar{3}m$) attempting to explain the diffraction data [5]. To fulfil the stoichiometry requirements for δ-Bi_2O_3 within the fluorite prototype, 25% vacancies in the anion sublattice should be present. In figure 1 the so-called Sillén model is shown [5, 7]. Here, vacancies are ordered in either ⟨100⟩, ⟨110⟩ or ⟨111⟩ direction [5, 7]. Based on the recent state of the art *ab initio* calculations, the ⟨100⟩ type of vacancy ordering is energetically preferred [8, 9]. Further improvements over the Sillén model were achieved by structural analysis, *ab initio* calculations and classical molecular dynamics resulting in combined vacancy ordering in ⟨110⟩ and ⟨111⟩ directions [10].

[3] Author to whom any correspondence should be addressed.

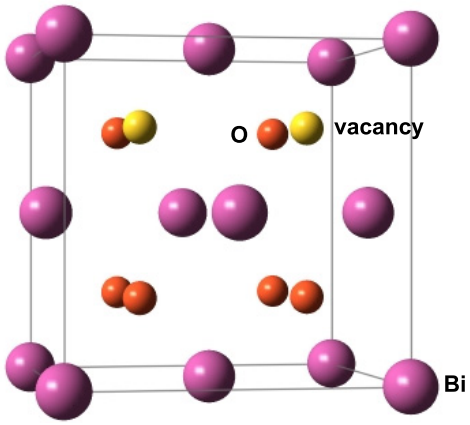

Figure 1. Sillén model for the structure of δ-Bi_2O_3. 25% of vacancies present in the fluorite prototype are ordered in the [010] direction.

We term this herein the modified Sillén model. Beside the Sillén model, there are two more structural models proposed by Gattow [11] and Willis [12]. The Gattow model essentially implies that six oxygen atoms are randomly distributed over the eight possible sites within the fluorite structure [11]. The Willis model is based on the experimental determination that δ-Bi_2O_3 could not be described by the ideal fluorite structure, rather, the oxygen atoms are displaced from their regular sites towards the centres of the interstitial positions [12]. Unlike the Sillén model, both the Gattow and the Willis model remain relatively unexplored in terms of *ab initio* modelling. For instance, randomness was considered by Zhukov *et al*, but relatively small cells were used and no statistical description of randomness was provided [13]. Systematic studies of δ-Bi_2O_3 structure, in particular randomness thereof, still lack in literature.

In this work, we systematically study the structure of δ-Bi_2O_3 probing ⟨100⟩ (the Sillén model) and combined ⟨110⟩ and ⟨111⟩ vacancy ordering (the modified Sillén model), random distribution of vacancies (the Gattow model) as well as local relaxations in the fluorite prototype (the Willis model) using *ab initio* calculations. The random distribution of vacancies is carried out by building ad hoc supercells and by using two different implementations of special quasirandom structures (SQS) [14]. We find that the combined ⟨110⟩ and ⟨111⟩ oxygen vacancy ordering is the most stable configuration. This can be understood based on the bonding analysis. Electron lone-pair charges in the predominantly ionic Bi–O matrix may stabilize the combined ⟨110⟩ and ⟨111⟩ oxygen vacancy ordering.

2. Computational details

Calculations in this work were carried out using density functional theory [15], as implemented in the Vienna *ab initio* simulation package (VASP), wherein the ultrasoft pseudopotentials with the generalized-gradient approximation are employed [16, 17]. All data were obtained by the VASP code, while additional codes were used to create input files (random supercells) and analyse the electronic structure, as described below. The following parameters were applied: convergence criterion for the total energy of 0.01 meV, Blöchl corrections for the total energy [18] cutoff of 500 eV, integration in the Brillouin zone according to Monkhorst–Pack [19] with $3 \times 3 \times 3$ irreducible k-points. The convergence tests were carried out in a previous work [9]. $2 \times 2 \times 2$ supercells containing 80 atoms (96 sites) were relaxed with respect to atomic positions and cell volumes. The same supercell size was used in previous works [9, 10]. Energy of formation was calculated with respect to elements: Bi with the α-As prototype, space group $R\bar{3}m$, and O as a free O_2 molecule with broken periodic boundary conditions. All phase stability data were obtained by VASP. Bulk moduli were obtained by fitting the energy–volume curves using the Birch–Murnaghan equation of states [20]. The elastic constants (C_{11}, C_{12}, C_{44}) were calculated using tetragonal and monoclinic strains applied to relaxed structures [21]. In order to study the bonding, electron density distributions, density of states (DOS) and Mulliken populations [22] were calculated. Here, the effective charge is referred to as a difference between the charge of a neutral atom and the total charge it possesses in a compound [23]. The effective charge, based on the Mulliken analysis, was obtained using the OpenMX code [24].[4] This code is also based on the density functional theory [15] and basis functions are implemented in the form of linear combination of localized pseudoatomic orbitals [25]. The electronic potentials were fully relativistic pseudopotentials with partial core corrections [26, 27] and the generalized-gradient approximation was applied [28]. The basis functions used were generated by a confinement scheme [25, 29] and specified as follows: Bi 5.0-s1p2d1 and O 4.5-s2p1. The first symbol designates the chemical name, followed by the cutoff radius (in Bohr radius) in the confinement scheme and the last set of symbols defines primitive orbitals applied. The energy cutoff (150 Ryd) and k-point grid ($1 \times 1 \times 1$) within the real space grid technique [30] were adjusted to reach the accuracy of 10^{-6} H/atom. An electronic temperature of 700 K is used to count the number of electrons within the Fermi–Dirac distribution. In our previous work [31], we studied the Mulliken effective charges of boron-rich solids using the OpenMX code and achieved a consistency with other Mulliken implementations based on the orthogonalized linear combination of atomic orbitals as well as the Hartree–Fock method [32].

For the Sillén model, the supercell was built based on the data by Carlsson and co-workers, thus exhibiting ⟨100⟩ ordering [9]. The modified Sillén model with combined ⟨110⟩ and ⟨111⟩ ordering was introduced from literature [10]. The description of randomness was herein carried out with a special care. Three types of supercells were built: ad hoc as well as two supercells based on different SQS implementations [14, 33]. Firstly, correlation functions were used to describe the randomness and secondly, the short range order (SRO) parameter was applied. The SQS implementation via correlation functions is available in the alloy theoretical automated toolkit (ATAT) [34–36]. Based

[4] OpenMX version 3.4 was used in this work and is available at www.openmx-square.org.

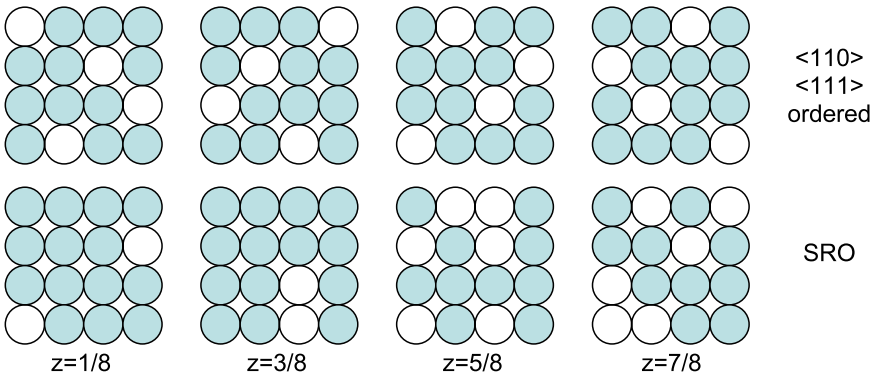

Figure 2. Stacking of the oxygen sublattice along [001] direction (z-value) in the $2 \times 2 \times 2$ supercell used for the modified Sillén model and the SRO based structure. Open and filled circles designate vacancies and oxygen atoms, respectively.

Table 1. Definition of relevant figures considered for the SQS description of δ-Bi_2O_3. Vertices of figures are given as fractional coordinates for $2 \times 2 \times 1$ supercell (48 sites).

Type	Multiplicity	Designation	Vertices		
Singlet	2	(1, 1)	(1/4, 1/4, 1/4)		
Singlet	1	(1, 2)	(0, 0, 0)		
Doublet	8	(2, 1)	(1/4, 1/4, 1/4)	(1/2, 1/2, 0)	
Doublet	6	(2, 2)	(3/4, 3/4, 3/4)	(1/4, 3/4, 3/4)	
Doublet	6	(2, 3)	(0, 0, 0)	(0, 1/2, 1/2)	
Doublet	12	(2, 4)	(3/4, 3/4, 3/4)	(1/4, 1/4, 3/4)	
Triplet	12	(3, 1)	(3/4, 3/4, 3/4)	(1/2, 1/2, 0)	(1/4, 3/4, 3/4)

Table 2. Pair and multisite correlation functions of the SQS structures used.

Figure	Random	SQS48-1	SQS48-2	SQS48-3
(1, 1)	−0.500 00	−0.500 00	−0.500 00	−0.500 00
(1, 2)	−1.000 00	−1.000 00	−1.000 00	−1.000 00
(2, 1)	0.500 00	0.500 00	0.500 00	0.500 00
(2, 2)	0.250 00	0.250 00	0.333 33	0.250 00
(2, 3)	1.000 00	1.000 00	1.000 00	1.000 00
(2, 4)	0.250 00	0.250 00	0.229 17	0.250 00
(3, 1)	−0.250 00	−0.250 00	−0.333 33	−0.250 00

Table 3. Short range order parameter for the oxygen sublattice of δ-Bi_2O_3.

Coordination shell	Short range order parameter
1	0.000 000 00
2	0.000 000 00
3	0.000 000 00
4	0.000 000 00
5	−0.041 666 67
6	−0.083 333 33
7	0.111 111 11
8	0.044 444 44
9	0.000 000 00
10	0.000 000 00

on the input space group ($Fm\bar{3}m$), the ATAT code provided all symmetrically distinct clusters: singlets, doublets and triplets. For each cluster correlation functions were defined to match a statistically random configuration. The correlation functions were based on trigonometric functions with specified dimensionality of the system and occupancy. Using these clusters together with their calculated multiplicity and size, all possible SQS supercells were generated having the specified space group and the composition. Table 1 contains the definition of relevant figures used to define the SQS supercell. 48 site supercells were built due to large computational demand. In table 2, the pair and multisite correlation functions of the SQS structure presented in table 1 are compared with those of the corresponding random structure. In the order of 6000 supercells were considered. Using the correlation functions from table 2, that best mimic random distribution of oxygen vacancies, 96 site supercell (80 atoms) was created from SQS48-1 and SQS48-3. This supercell is henceforth termed SQS96. The selection criterion for reducing these 6000 configurations to the three listed in table 2 was minimizing the difference between the values of the correlation functions of the statistically random configuration and the here-considered SQS configurations. Furthermore, the SQS implementation via SRO parameter is available within the locally self-consistent Green's function (LSGF) software package [37, 38]. The LSGF code is based on the Dyson equation for cluster Green's functions [37, 38]. Here, this code is only used to generate SQS supercells. Warren–Cowley SRO parameter [39] within three coordination shells was used to account for randomness in the oxygen sublattice and the exact values for ten coordination shells for δ-Bi_2O_3 are provided in table 3. This supercell is henceforth termed SRO. The SQS configurations generated by the ATAT and LSGF codes were used as input for the VASP code. Figure 2 shows the stacking of the oxygen atoms and vacancies in δ-Bi_2O_3 for the modified Sillén model and the SRO supercell.

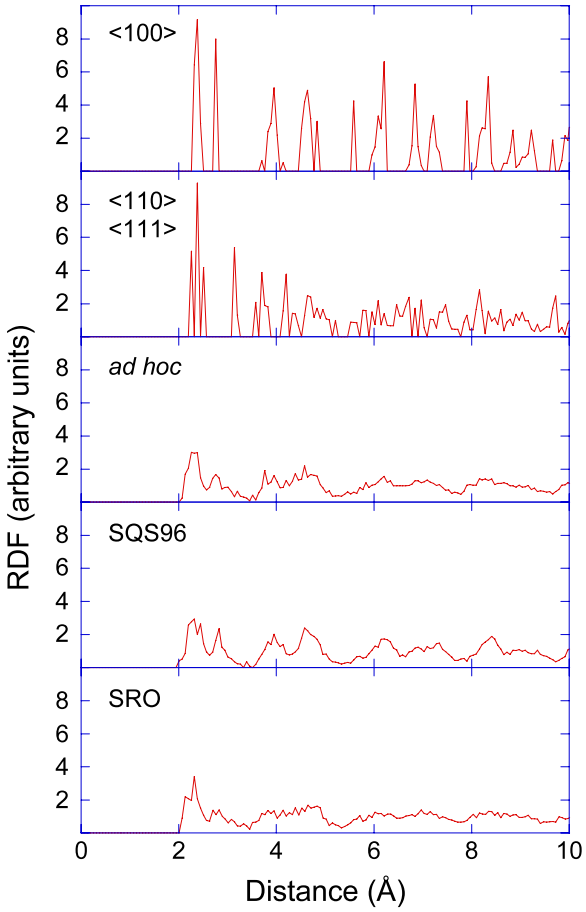

Figure 3. Radial distribution functions (RDF) for δ-Bi_2O_3 with $\langle 100\rangle$ vacancy ordering, combined $\langle 110\rangle$ and $\langle 111\rangle$ vacancy ordering, ad hoc random distribution of vacancies and two SQS configurations: SQS96 (randomness defined by correlation functions) as well as SRO (randomness defined by SRO parameter).

3. Results and discussion

Table 4 contains the calculated lattice parameters, energies of formation, bulk moduli and elastic constants (C_{11}, C_{12}, C_{44}) for δ-Bi_2O_3 described using the Sillén model ($\langle 100\rangle$ vacancy ordering), the modified Sillén model (combined $\langle 110\rangle$ and $\langle 111\rangle$ vacancy ordering), ad hoc random distribution of vacancies and two SQS implementations: SQS96 (randomness defined by correlation functions as given in tables 1 and 2) as well as SRO (randomness defined by SRO parameter as provided in table 3). The lattice parameter ranges from 5.577 Å for the $\langle 100\rangle$ vacancy ordering to 5.659 Å for the SQS96 random distribution of vacancies. The latest structural refinement with the Rietveld method using the neutron diffraction data yielded the lattice parameter of 5.6549(9) Å [40]. This accounts for 1.4% and 0.1% deviation for the $\langle 100\rangle$ vacancy ordering and the SQS96 random distribution, respectively. Even though the lattice parameter for the random distribution of oxygen vacancies appears to agree better with the experimental data, this is within standard *ab initio* precision. Similar argumentation holds for the bulk moduli ranging from 108 to 118 GPa. Furthermore, the conditions that $C_{11} - C_{12} > 0$ and $C_{44} > 0$ hold, implying

Table 4. Lattice parameter (a), energy of formation with respect to elements (E_f), bulk modulus (B) and all elastic constants (C_{11}, C_{12}, C_{44}) for δ-Bi_2O_3. Five structural models are considered.

	a (Å)	E_f (eV/atom)	B (GPa)	C_{11} (GPa)	C_{12} (GPa)	C_{44} (GPa)
$\langle 100\rangle$	5.577	−1.478	111.8	189.7	72.9	52.1
$\langle 110\rangle\langle 111\rangle$	5.602	−1.572	118.3	169.3	92.8	62.5
ad hoc	5.604	−1.561	112.0	177.7	79.1	60.0
SQS96	5.659	−1.555	107.8	173.9	74.7	55.3
SRO	5.641	−1.552	109.1	166.5	80.4	60.5

that all configurations are stable with respect to elastic homogeneous deformations. Based on the energy of formation, the structural model for δ-Bi_2O_3 can be distinguished. It is conclusive that the $\langle 100\rangle$ vacancy ordering is the least stable with the energy of formation of −1.478 eV/atom, while the configuration with the combined $\langle 110\rangle$ and $\langle 111\rangle$ vacancy ordering is the most stable with −1.572 eV/atom. We also probed the influence of a tetragonal distortion on the energy of formation for the $\langle 100\rangle$ configuration, as suggested in [8], and find a minor stability increase of 6 meV/atom. The models with random distribution of oxygen vacancies are rather close to the configuration with the combined $\langle 110\rangle$ and $\langle 111\rangle$ vacancy ordering; they are only 12–20 meV/atom less stable. It appears that the modified Sillén model is the groundstate of δ-Bi_2O_3, which is consistent with *ab initio* and neutron diffraction data in [10]. However, this difference in the energy of formation between the modified Sillén model and the random configurations may be overcome during vapour phase condensation experiments, as exemplified by metastable cubic $Ti_{1-x}Al_xN$ [41], $Cr_{1-x}Al_xN$ [42] and Cu–Mo [43]. Furthermore, it is reasonable to assume that these small energy differences may be overcome at elevated temperatures due to entropic contributions to the total energy.

The structural models for δ-Bi_2O_3 are further analysed by calculating the radial distribution functions (RDF) thereof, which enables direct comparison with future experiments. Figure 3 contains RDF for δ-Bi_2O_3 based on the Sillén model ($\langle 100\rangle$ vacancy ordering), the modified Sillén model (combined $\langle 110\rangle$ and $\langle 111\rangle$ vacancy ordering), the ad hoc random distribution of vacancies and two SQS implementations: SQS96 (randomness defined by correlation functions) as well as SRO (randomness defined by SRO parameter). The first RDF peak(s) at approximately 2.3–2.5 Å corresponds to the Bi–O bond lengths in the first coordination shell. These RDF data can be classified as discrete (ordered configurations) and continuous (random configurations). It is important to note that the continuous RDF does not imply that any of these configurations mimic an amorphous state. The RDF for the amorphous state is typically depicted by continuous population superimposed on a relatively large background [31, 44, 45], which is not the case here. We suggest that the underlying reason for the classification of the RDF data is the local structural relaxations, in agreement with the Willis model [12]. In order to support this notion, we have analysed the relative local structural relaxations for two configurations: combined $\langle 110\rangle$ and $\langle 111\rangle$ vacancy ordering as well as the SRO configuration. For both of these configurations, there are

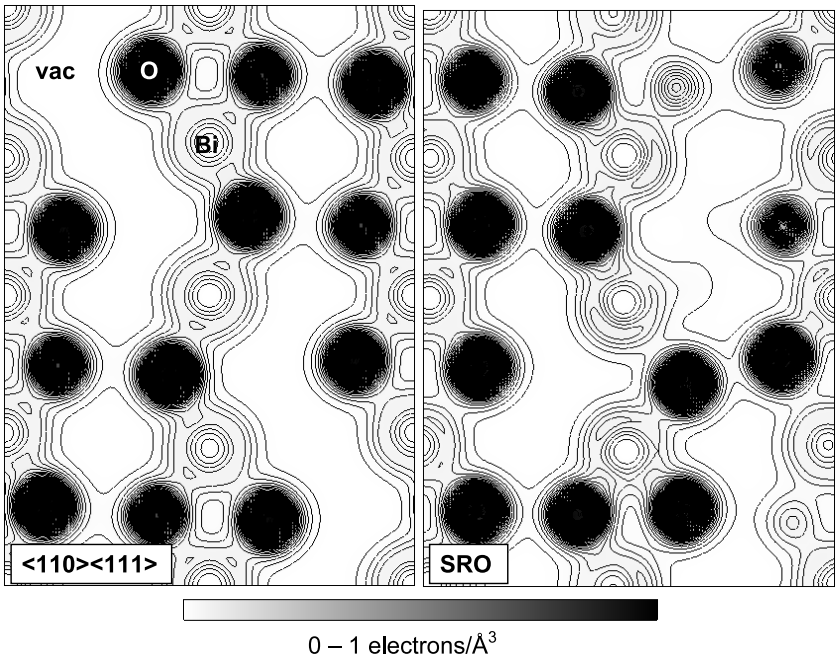

Figure 4. Electron density distribution in the (110) plane for two configurations: combined ⟨110⟩ and ⟨111⟩ oxygen vacancy ordering as well as random vacancy distribution with oxygen vacancies described with the SRO parameter.

smaller Bi relaxations in the order of 1.2%–6.7%. On the other hand, there are significant differences for the oxygen sublattice identified when these two configurations are compared. For the combined ⟨110⟩ and ⟨111⟩ vacancy ordering configuration, the O relaxations are 3.5%, while for the SRO configuration these are in the range from 1.4% to 28.6%. With larger local structural relaxations both in magnitude and spread, it may be anticipated that the RDF data are continuous, as observed. Furthermore, it is expected that diffraction based methods may be able to distinguish between these two RDF types since the experimental RDF analysis was shown to pinpoint stages of crystallization [46, 47].

In order to characterize the bonding in the configurations probed and shed some light on the phase stability, we study the electron density distribution in the (110) plane of the $2 \times 2 \times 2$ supercell for two δ-Bi_2O_3 representatives: combined ⟨110⟩ and ⟨111⟩ oxygen vacancy ordering as well as the SRO configuration (see figure 4). It is apparent that the most dominating bonding is of the ionic character due to charge transfer from Bi to O. These data are consistent with literature [8, 10]. Based on the Mulliken analysis, the effective charge for Bi and O for the configuration with the combined ⟨110⟩ and ⟨111⟩ oxygen vacancy ordering is 1.18 and −0.78, respectively. On the other hand, the SRO configuration exhibits a distribution of effective charges, being from 0.85 to 1.29 and from −0.74 to −0.82 for Bi and O, respectively. Clearly, some differences in the chemical bonding are present. In the configuration with the combined ⟨110⟩ and ⟨111⟩ oxygen vacancy ordering, two types of Bi local environments can be observed: uniform distribution of electron lone-pair charge of Bi and directed electron lone-pair charge of Bi towards vacancies. On the other hand, the SRO configuration exhibits only directed electron lone-pair charge of Bi towards vacancies. A more detailed analysis of the electronic structure of these two δ-Bi_2O_3 representatives (combined ⟨110⟩ and ⟨111⟩ oxygen vacancy ordering and the SRO configuration) is provided through the DOS data as shown in figure 5. There are several general remarks that can be made. Firstly, we observe that both δ-Bi_2O_3 representatives exhibit a band gap around 2 eV. Secondly, these phases may be ionically bonded and several DOS regions may be distinguished: Bi s states (approximately −10 to −8 eV), Bi p–O p strongly hybridized states (approximately −5 to −2 eV) and Bi s–O p weakly hybridized states with some contribution of Bi p orbitals (approximately −2 to 0 eV). Based on the crystal orbital overlap population analysis [8], the DOS region from −2 to 0 eV produces Bi lone pairs and is a result from the mixing of the antibonding Bi s and O p states with Bi p orbitals. There is a distinction between these two representatives with respect to the Bi lone pairs. Stronger antibonding is present in the SRO configuration as compared to the configuration with combined ⟨110⟩ and ⟨111⟩ oxygen vacancy ordering. This may explain the stability differences observed since antibonding is likely to decrease the phase stability. We also speculate that this well-defined and narrow peak in the DOS of the SRO configuration may imply a pronounced directionality of the Bi lone pairs as discussed above in conjunction with figure 4. It is known that electron lone-pair charges in Bi-containing compounds are responsible for structural stabilizations [48]. The combined ⟨110⟩ and ⟨111⟩ oxygen vacancy ordered configuration may thus be slightly preferred over the random counterparts.

4. Conclusions

We have systematically studied the structure of δ-Bi_2O_3 probing ⟨100⟩ (the Sillén model) and combined ⟨110⟩ and

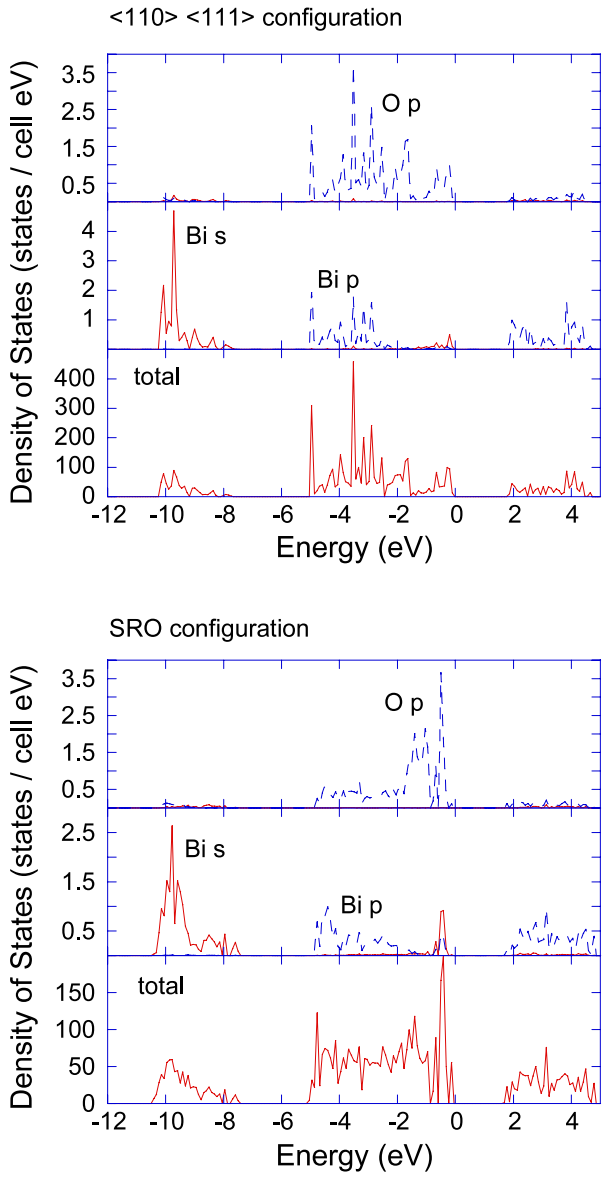

Figure 5. Total and partial density of states for two configurations: combined ⟨110⟩ and ⟨111⟩ oxygen vacancy ordering as well as random vacancy distribution with oxygen vacancies described with the SRO parameter. The data were obtained using the VASP code. The Fermi level is set to zero.

⟨111⟩ oxygen vacancy ordering (the modified Sillén model), random distribution of oxygen vacancies (the Gattow model) as well as local relaxations in the fluorite prototype (the Willis model) using *ab initio* calculations. The random distribution of vacancies is carried out by building ad hoc supercells and by using two different implementations of SQS: SQS96 and SRO. We find that the combined ⟨110⟩ and ⟨111⟩ oxygen vacancy ordering is the most stable configuration and that the models with random distribution of oxygen vacancies are 12–20 meV/atom less stable, which may be overcome in vapour phase condensation experiments. RDF can be classified as discrete (ordered configurations) and continuous (random configurations). This can be understood based on local structural relaxations. Up to 28.6% relative local relaxation of the oxygen sublattice is present in the random configurations giving rise to continuous RDF. The obtained phase stability is consistent with the bonding analysis. Electron lone-pair charges in the predominantly ionic Bi–O matrix may stabilize the combined ⟨110⟩ and ⟨111⟩ oxygen vacancy ordering.

Acknowledgment

This work was financially supported by the Deutsche Forschungsgemeinschaft (DFG) within the project Schn 735/14-1.

References

[1] Goodenough J B 2000 *Nature* **404** 821
[2] Huang H, Nakamura M, Su P, Fasching R, Saito Y and Prinz F B 2007 *J. Electrochem. Soc.* **154** B20
[3] Boivin J C and Mairesse G 1998 *Chem. Mater.* **10** 2870
[4] Azad A M, Larose S and Akbar S A 1994 *J. Mater. Sci.* **29** 4135
[5] Sammes N M, Tompsett G A, Näfe H and Aldinger F 1999 *J. Eur. Ceram. Soc.* **19** 1801
[6] Switzer J A, Shumsky M G and Bohannan E W 1999 *Science* **284** 293
[7] Sillén L G 1937 *Ark. Kemi Mineral. Geol.* **12A** 1
[8] Walsh A, Watson G W, Payne D J, Edgell R G, Guo J, Glans P-A, Learmonth T and Smith K E 2006 *Phys. Rev.* B **73** 235104
[9] Carlsson J M, Hellsing B, Domingos H S and Bristowe P D 2002 *Phys. Rev.* B **65** 205122
[10] Aidhy D S, Nino J C, Sinnott S B, Wachsman E D and Phillpot S R 2008 *J. Am. Ceram. Soc.* **91** 2349
[11] Gattow G and Schröder H 1962 *Z. Anorg. Allg. Chem.* **318** 176
[12] Willis B T M 1965 *Acta Crystallogr.* **18** 75
[13] Zhukov V P, Zhukovskii V M, Zainullina V M and Medvedeva N I 1999 *J. Struct. Chem.* **40** 831
[14] Zunger A, Wei S-H, Ferreira L G and Bernard J E 1990 *Phys. Rev. Lett.* **65** 353
[15] Hohenberg P and Kohn W 1964 *Phys. Rev.* B **136** 864
[16] Kresse G and Hafner J 1993 *Phys. Rev.* B **48** 13115
[17] Kresse G and Hafner J 1994 *Phys. Rev.* B **49** 14251
[18] Blöchl P E 1994 *Phys. Rev.* B **50** 17953
[19] Monkhorst H J and Pack J D 1976 *Phys. Rev.* B **13** 5188
[20] Birch F 1978 *J. Geophys. Res.* **83** 1257
[21] Liu A Y and Singh D J 1993 *Phys. Rev.* B **47** 8515
[22] Mulliken R S 1955 *J. Chem. Phys.* **23** 1833
[23] Allred A L and Rochow E G 1958 *J. Inorg. Nucl. Chem.* **5** 264
[24] Ozaki T and Kino H 2005 *Phys. Rev.* B **72** 045121
[25] Ozaki T 2003 *Phys. Rev.* B **67** 155108
[26] Troullier N and Martins J L 1991 *Phys. Rev.* B **43** 1993
[27] Blöchl P E 1990 *Phys. Rev.* B **41** 5414
[28] Perdew J P, Burke K and Ernzerhof M 1996 *Phys. Rev. Lett.* **77** 3865
[29] Ozaki T and Kino H 2004 *Phys. Rev.* B **69** 195113
[30] Soler J M, Artacho E, Gale J D, Garcia A, Junquera J, Ordejon P and Sanchez-Portal D 2002 *J. Phys.: Condens. Matter* **14** 2745
[31] Music D and Schneider J M 2008 *J. Phys.: Condens. Matter* **20** 195203
[32] Li D and Ching W Y 1996 *Phys. Rev.* B **54** 1451
[33] Ruban A V and Abrikosov I A 2008 *Rep. Prog. Phys.* **71** 046501
[34] van de Walle A and Ceder G 2002 *J. Phase Equilib.* **23** 348
[35] van de Walle A and Asta M 2002 *Modelling Simul. Mater. Sci. Eng.* **10** 521
[36] van de Walle A, Asta M and Ceder G 2002 *CALPHAD* **26** 539

[37] Abrikosov I A, Niklasson A M N, Simak S I, Johansson B, Ruban A V and Skriver H L 1996 *Phys. Rev. Lett.* **76** 4203
[38] Abrikosov I A, Simak S I, Johansson B, Ruban A V and Skriver H L 1997 *Phys. Rev.* B **56** 9319
[39] Cowley J M 1950 *J. Appl. Phys.* **21** 24
[40] Yashima M and Ishimura D 2003 *Chem. Phys. Lett.* **378** 395
[41] Mayrhofer P H, Music D and Schneider J M 2006 *J. Appl. Phys.* **100** 094906
[42] Mayrhofer P H, Music D, Reeswinkel Th, Fuß H-G and Schneider J M 2008 *Acta Mater.* **56** 2469
[43] Gong H R, Kong L T and Liu B X 2004 *Phys. Rev.* B **69** 024202
[44] Music D, Kreissig U, Chirita V, Schneider J M and Helmersson U 2003 *J. Appl. Phys.* **93** 940
[45] Alvarez F and Valladares A A 2003 *Solid State Commun.* **127** 486
[46] Mattern A, Moldenhauser S, Danzig A, Blau W, Richter K and Müller M 1993 *Phys. Status Solidi* a **138** 59
[47] Wei S, Li Z, Yin S, Zhang X, Liu W and Wang X 2001 *J. Synchrotron Radiat.* **8** 566
[48] Seshadri R and Hill N A 2001 *Chem. Mater.* **13** 2892